Oxidative Phosphorylation Flexibility in the Liver of Mice Resistant to High-Fat Diet–Induced Hepatic Steatosis

Carinne Poussin,[1] Mark Ibberson,[1,2] Diana Hall,[1] Jun Ding,[1] Jamie Soto,[3] E. Dale Abel,[3] and Bernard Thorens[1]

OBJECTIVE—To identify metabolic pathways that may underlie susceptibility or resistance to high-fat diet–induced hepatic steatosis.

RESEARCH DESIGN AND METHODS—We performed comparative transcriptomic analysis of the livers of A/J and C57Bl/6 mice, which are, respectively, resistant and susceptible to high-fat diet–induced hepatosteatosis and obesity. Mice from both strains were fed a normal chow or a high-fat diet for 2, 10, and 30 days, and transcriptomic data were analyzed by time-dependent gene set enrichment analysis. Biochemical analysis of mitochondrial respiration was performed to confirm the transcriptomic analysis.

RESULTS—Time-dependent gene set enrichment analysis revealed a rapid, transient, and coordinate upregulation of 13 oxidative phosphorylation genes after initiation of high-fat diet feeding in the A/J, but not in the C57Bl/6, mouse livers. Biochemical analysis using liver mitochondria from both strains of mice confirmed a rapid increase by high-fat diet feeding of the respiration rate in A/J but not C57Bl/6 mice. Importantly, ATP production was the same in both types of mitochondria, indicating increased uncoupling of the A/J mitochondria.

CONCLUSIONS—Together with previous data showing increased expression of mitochondrial β-oxidation genes in C57Bl/6 but not A/J mouse livers, our present study suggests that an important aspect of the adaptation of livers to high-fat diet feeding is to increase the activity of the oxidative phosphorylation chain and its uncoupling to dissipate the excess of incoming metabolic energy and to reduce the production of reactive oxygen species. The flexibility in oxidative phosphorylation activity may thus participate in the protection of A/J mouse livers against the initial damages induced by high-fat diet feeding that may lead to hepatosteatosis. ***Diabetes*** **60:2216–2224, 2011**

Development of hepatic steatosis results from an impaired balance between hepatocyte fatty acid uptake, catabolism, lipogenesis, and export in the form of VLDL-associated triglycerides (1). Fat accumulation in liver is often associated with insulin resistance and can trigger the development of inflammation and fibrosis. Many mechanisms can deregulate the balance between the lipid metabolic pathways that normally regulate hepatocyte lipid homeostasis. Some may be initiated locally by an altered inflammatory state of the liver (2,3) but could also be secondary to obesity. Indeed, adipose tissue expansion induces a local inflammatory response that attracts circulating leukocytes and leads to the production of cytokines by adipocytes and inflammatory cells (3–5). This results in adipose tissue insulin resistance and an increased release of free fatty acids, which together with the secreted cytokines can induce insulin resistance in muscle and liver. Deregulated liver metabolism or inflammatory pathways can also induce adipose tissue inflammation and whole body insulin resistance with increased susceptibility to the development of the metabolic syndrome (3,6).

The comparative study of animal models with different susceptibilities to develop fatty livers can provide interesting clues about the metabolic pathways involved in pathogenic processes (7). One important question, however, is at what stage of the pathogenic process should the mice be studied. Often, comparison of gene expression by microarray analysis is performed after several months of high-fat diet (HFD) feeding when the disease is fully established. Such an approach can describe the alterations associated with the disease at the stage investigated. However, it may be more relevant to study the initial response to the challenging conditions, as this may dictate the subsequent changes in gene expression that cause the final pathological phenotype.

In an earlier study, we compared the adaptation to HFD feeding for 2, 10, and 30 days of A/J (AJ) and C57Bl/6J (B6) mice (8). These mice are, respectively, resistant and sensitive to steatohepatitis and obesity; the AJ mice also exhibit a lower liver proinflammatory state than B6 mice. Transcript profiling showed that in the AJ mouse livers, both in the basal state and after HFD feeding, there was a higher expression of peroxisomal β-oxidation genes and of genes encoding microsomal enzymes that favor the production of 2-arachidonylglycerol (2-AG), an endocannabinoid that limits cytokine production by Kupffer cells (8).

Here, we reanalyzed these microarray data by performing time-dependent gene set enrichment analysis (GSEA). We observed that the steatosis-resistant AJ mice displayed a transient and coordinated upregulation of 13 oxidative phosphorylation (OxPhos) genes, which was not observed in the B6 mouse livers. Biochemical measurement of OxPhos activity confirmed that HFD feeding increased mitochondrial respiration in AJ liver mitochondria but this was uncoupled from ATP production. In contrast, in the livers of B6 mice, no change in respiration rate or uncoupling was observed. This indicates that the AJ mouse livers respond to HFD feeding by an adaptive response of their oxidative phosphorylation chain to increase energy dissipation and reduce reactive oxygen species production. Together with our previous study, the present one indicates

From the [1]Center for Integrative Genomics, University of Lausanne, Lausanne, Switzerland; the [2]Vital-IT Group, Swiss Institute of Bioinformatics, Lausanne, Switzerland; and the [3]Program in Molecular Medicine and Division of Endocrinology, Metabolism and Diabetes, University of Utah School of Medicine, Salt Lake City, Utah.

Corresponding author: Bernard Thorens, bernard.thorens@unil.ch.

Received 13 March 2011 and accepted 28 May 2011.

DOI: 10.2337/db11-0338

This article contains Supplementary Data online at http://diabetes.diabetesjournals.org/lookup/suppl/doi:10.2337/db11-0338/-/DC1.

that flexibility in the activation of several lipid metabolic pathways as well as OxPhos activity contributes to the resistance to HFD-induced liver metabolic deregulation.

RESEARCH DESIGN AND METHODS

Animals and diets. Diet-inducible obesity experiments were performed in B6 mice (Janvier, Les Oncins, France) and AJ mice (Jackson Laboratories, MD) as follows. After 1 week acclimatization, 4–5-week-old male B6 or AJ mice were fed with a normal chow (NC; Mouse/Rat elevage N°NAFAG 3436) or an HFD (Research Diet N°D12331 composed of 58% fat, 26% carbohydrates, 16% proteins) for 2, 10, and 30 days. After these different periods, mice were anesthetized by isoflurane inhalation and liver samples were collected, snap frozen in liquid nitrogen, and stored at −80°C. Body weight, blood glucose levels, and insulinemias were measured in some of these groups (Supplementary Fig. 1). Experimental groups included six mice per strain/diet/time point. Mice were housed at 12 h:12 h light:dark cycle. All animal studies were approved by the Institutional Animal Use and Care Committee of the University of Utah and by the Service Vétérinaire Cantonal from the Canton de Vaud.

RNA preparation, labeling, and hybridization on cDNA microarrays. RNA from six different mice per group was extracted from liver samples using the guanidinium thiocyanate method (9) followed by further purification on RNeasy columns (Qiagen, Hombrechtikon, Switzerland). RNA quality was checked before and after amplification using a bioanalyzer 2100 (Agilent, Basel, Switzerland). RNA samples were amplified from individual HFD-fed mice (six per time point) using MessageAmp (Ambion, Rotkreuz, Switzerland). Equal amounts of RNA from six mice fed for 2, 10, or 30 days on NC were pooled and amplified. Two differently labeled fluorescent probes (amplified individual RNA from liver of HFD mice labeled with Cy5 and amplified pools of RNA from NC mice labeled with Cy3) were prepared by indirect labeling according to published protocols (10). For each time point, individual Cy5-labeled amplified RNA and Cy3-labeled amplified RNA pools were hybridized on microarrays containing 17,664 spotted cDNAs (arrays were produced at the DNA Array Facility, University of Lausanne). Six technical replicates were performed, including three dye-swapping hybridizations. Scanning, image, and quality control analyses were performed as previously published (10). Data were expressed as $\log_2$ intensity ratios ($\log_2$[Cy5/Cy3] = M), normalized using print tip locally weighted linear (Lowess) regression (both within array and between array normalization was performed), and filtered based on spot quality. All analyses were performed using R and Bioconductor software (11).

Statistical analysis: gene filtering. A moderated *F* test was applied to remove genes that were not regulated at any time point during the experiment using the Limma package from Bioconductor (http://www.bioconductor.org). Empirical *P* values were calculated following a 10,000-label permutation procedure. Genes with an adjusted *P* value < 0.05 were selected for GSEA analysis. We applied GSEA to this expression matrix of filtered genes as described in the next section.

Time-course GSEA method. See also Supplementary Fig. 1 for an illustration of the method.

Defining "prototypes." According to the design of our microarray experiment, genes can be differentially expressed, at 2, 10, and 30 days between HFD and NC samples. Gene expression can increase (M >0), not be modified (M = 0), or decrease (M <0) at each time point. At day 0 (T0), the expression value was considered as 0 (ratio in $\log_2$). This led to 27 possibilities of theoretical gene expression behavior termed as "prototypes" (Supplementary Fig. 1). Each prototype was transformed into a vector with time point regulations coded as +1 (upregulation), 0 (no regulation), or −1 (downregulation). The prototype (0,0,0) was excluded.

Coding the gene expression matrix. From the gene expression matrix we encoded the regulation of each gene at each time point as +1, 0, or −1 according to overexpression, no regulation, or downregulation of HFD versus NC samples respectively.

Correlation calculation. Pearson correlation between the i^{th} prototype and each/every gene from the expression matrix was calculated.

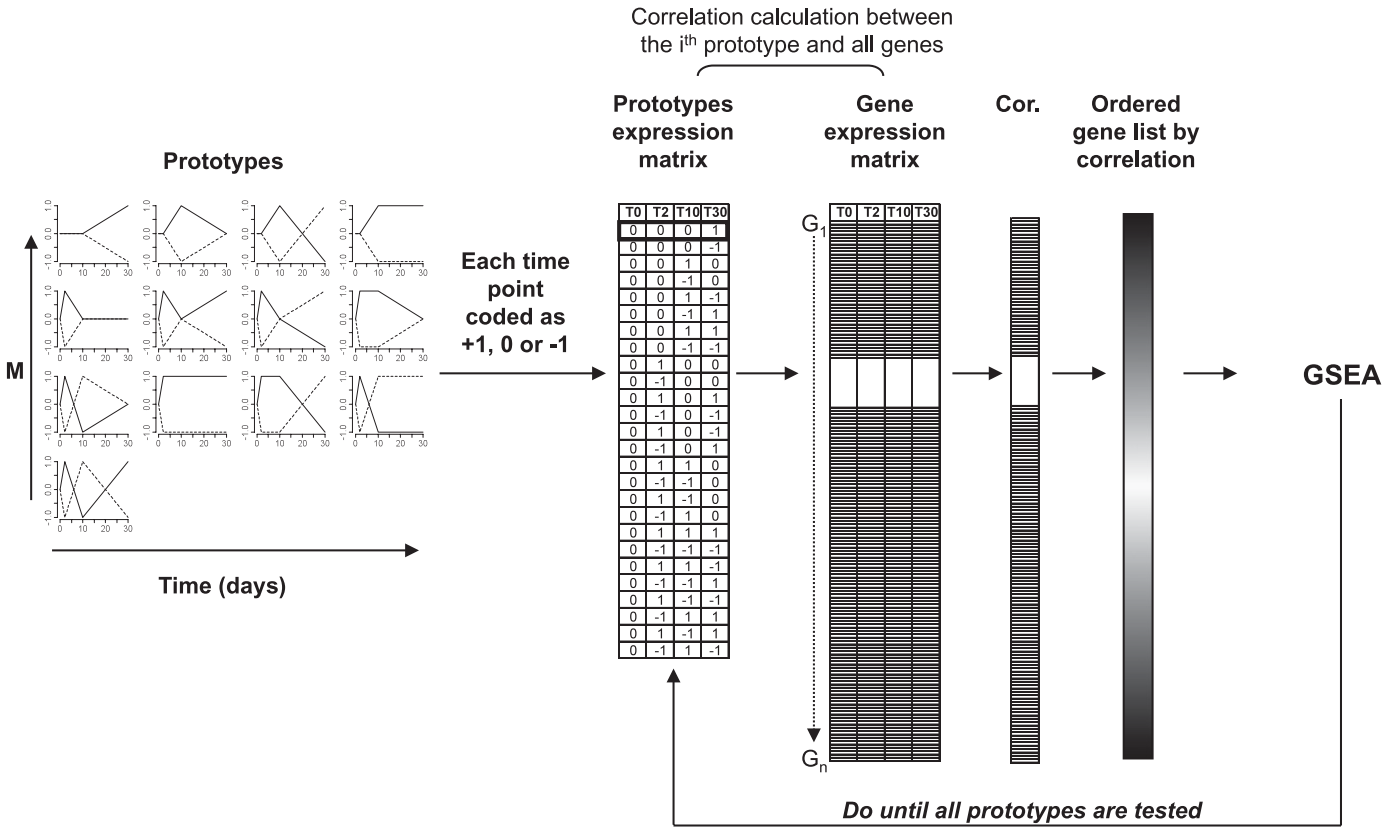

FIG. 1. Schematic of our time-course GSEA method. "Prototypes" are created as theoretical gene expression behaviors across the HFD time course. The prototype expression matrix is produced by coding each time point of a given prototype with a value of +1, 0, or −1. The gene expression matrix is the regulation of each gene at each time point, coded as +1, 0, or −1 according to overexpression, no regulation, or downregulation of HFD vs. NC samples, respectively. The correlation vector is generated by calculating the Pearson correlation between the i^{th} prototype and all genes present in the expression matrix. Genes are then ordered based on their correlation values. GSEA is performed using MSigDB gene sets. The procedure is repeated until all prototypes are tested. At the end of the procedure, a list of significant gene sets associated with each prototype is obtained as output, which could be considered as biological function–associated clusters of genes.

Gene ordering. Genes were then ordered based on correlation values. Genes highly correlated or anticorrelated with the i^{th} prototype were ranked at the top and at the bottom of the gene list, respectively.

GSEA. On this list of ranked genes, we performed GSEA using the MSigDB database as a source of gene sets (12,13). Since the gene sets contained human gene identifiers, the genes in each gene set were translated into the corresponding mouse gene symbol using the Homologene database at National Center for Biotechnology Information. In brief, for each gene set, GSEA statistically assesses whether the top or the bottom of the ranked list is enriched in genes belonging to a particular gene set. In order to put more weight on genes highly correlated or anticorrelated with the i^{th} prototype and to obtain genes with similar expression patterns, the "weight" parameter p, involved in the calculation of the enrichment score, was set to 2. Estimation of enrichment score significance for each gene set was obtained using a 1,000-label permutation procedure.

Output. The whole procedure was repeated until all prototypes were tested. A list of significant gene sets associated with each prototype was obtained as output. For these gene sets, genes corresponding to the leading edge subset (genes that contribute to the maximum enrichment score) constitute the biological function–associated clusters. Gene sets with a false discovery rate (FDR) <0.25 (12) and a number of leading edge subset of genes 4 passed selection criteria.

Expression analysis of OxPhos genes. Log_2 fold-change expression values for OxPhos genes were extracted for HFD versus NC-fed AJ and B6 mice at each time point (six mice per time point) using KEGG annotation (KEGG pathway mmu00190). Mean centroid expression values were calculated by first scaling the data to a mean of zero and unit SD across all samples, and then calculating the average expression across all OxPhos genes for each sample (9).

Measurement of ATP and oxygen consumption in isolated liver mitochondria. Mitochondrial oxygen consumption and ATP production were measured using techniques described previously (14). Mitochondria were isolated from livers of B6 and AJ mice after 0 or 10 days of HFD or NC, respectively. Mice were killed by cervical dislocation. The livers were immediately placed in ice-cold STE buffer (250 mmol/L sucrose, 5 mmol/L Tris, 2 mmol/L EGTA at pH 7.4) and cut into small pieces. Samples were homogenized and mitochondria were isolated, using protocols previously described by us (15). Rates of oxygen consumption by mitochondria were measured with a FOXY-*R*-AF probe (Ocean Optics Inc, Dunedin, FL), using the substrates 0.02 mmol/L palmitoyl carnitine (PC) and 5 mmol/L malate, or 5 mmol/L succinate and 0.01 mmol/L rotenone, as previously described (15). ATP concentration was determined by a bioluminescence assay, based on the luciferin/luciferase reaction, with the ATP assay kit (ThermoLabsystems, Issy-les-Moulineaux, France).

RESULTS

OxPhos genes are coordinately upregulated in HFD-fed AJ mice. To detect early transcriptional events associated with, and possibly causing, the differential susceptibility of AJ and B6 mice to the development of hepatic steatosis and obesity, we compared global gene expression in the livers of these mice fed NC or HFD for 2, 10, and 30 days. To identify sets of coordinately regulated genes that might have escaped our previous analysis (8), we reanalyzed our data using time-series GSEA.

GSEA measures the extent to which members of a particular gene set are enriched in the top or bottom of a list of ranked expression values (12,13). Here, in order to take into account time-series data, we first created prototype profiles representing different gene expression behaviors over the three time points of our study and ranked the genes according to their correlation with each of these profiles to create gene lists (see Fig. 1 and RESEARCH DESIGN AND METHODS for details). GSEA was then used to identify pathways that were significantly enriched for genes in each of these gene lists. Here, significant enrichment indicates that genes belonging to a particular pathway showed a similar expression profile over the three time points of our study.

Using this method, we identified 16 out of a total of 522 gene sets that were enriched for gene expression profiles from HFD-fed AJ mice, 8 of which are related to mitochondrial metabolism (Fig. 2, indicated by asterisks). Among these gene sets, three are related to electron

		AJ							B6							
Gene set name (Enrichment)	N	N_m	N_{le}	FDR	Gene expression pattern (median)			Nb genes B6 vs AJ >0	Nb genes B6 vs AJ <0	Nb genes B6 vs AJ =0	N_m	N_{le}	FDR	Gene expression pattern (median)			Nb genes B6 vs AJ >0	Nb genes B6 vs AJ <0	Nb genes B6 vs AJ =0
					T2	T10	T30							T2	T10	T30			
CR_SIGNALLING	198	7	4	0.15				0	1	3									
TCA	15	7	4	0.09				2	0	2									
Krebs-TCA_cycle	36	7	4	0.18				2	0	2									
insulin_signalling	103	7	5	0.21				2	1	2									
INSULIN_2F_UP	235	15	11	0.18				4	1	6									
human_mitoDB_6_2002	428	35	19	0.22				14	1	4	77	50	0.092				16	13	21
mitochondr	447	38	27	0.13				18	4	5	68	18	0.16				3	9	6
VOXPHOS	87	15	13	0.20				13	0	0									
Electron_Transport_Chain	110	14	12	0.18				12	0	0									
MAP00190_Oxidative_Phosphorylation	63	8	6	0.22				5	1	0									
PGC	425	33	29	0.23				15	7	0	65	29	0.18				5	11	13
Peroxisome	37	6	5	0.17				1	2	2									
RAP_DOWN	229	27	24	0.23				12	3	9	48	32	0.06				11	3	18
GLUT_DOWN	313	28	25	0.19				12	7	6	57	37	0.057				12	5	20
LEU_DOWN	180	21	16	0.24				9	4	3									
GLUT_UP	296	9	6	0.24				1	2	3									
PROLIF_GENES	394										41	21	0.071				6	8	7
p53_signalling	101										14	7	0.17				2	3	2
ANDROGEN_UP_GENES	86										9	4	0.022				0	1	3
igf1Pathway	20										6	4	0.121				0	0	4
il6Pathway	21										8	4	0.14				0	0	4
CR_PROTEIN_MOD	150										17	9	0.157				1	2	6
RAR_UP	49										10	4	0.22				1	3	0

up
down
not modulated

FIG. 2. Gene sets identified by time-course GSEA in HFD-fed AJ and B6 mice. Significantly enriched gene sets (FDR <0.25; N_{le} ^{3}4) from time-course GSEA analysis of HFD-fed AJ and B6 mice. See Supplementary Table 1 for a description of the gene sets. The different columns of the table correspond to the following: N, total number of genes present in the gene set; N_m, number of genes from the gene set present in the gene list; N_{le}, number of genes that contribute to the maximum enrichment score (leading edge genes) for a given gene set; FDR, false discovery rate; Gene expression pattern, color coding of the median expression of the leading edge genes (green, downregulation; gray, no regulation; red, upregulation); Nb genes B6 vs. AJ >0, number of genes whose log_2 expression level ratio between B6 and AJ mice (at basal level) is positive, meaning that the mRNA level is higher in B6 than in AJ mice; Nb genes B6 vs. AJ <0, number of genes whose log_2 expression level ratio between B6 and AJ mice (at basal level) is negative, meaning that the mRNA level is higher in AJ than in B6 mice; Nb genes B6 vs. AJ = 0, number of genes whose log_2 expression level ratio between B6 and AJ mice (at basal level) is 0, meaning that the mRNA level is the same between AJ and B6 mice.

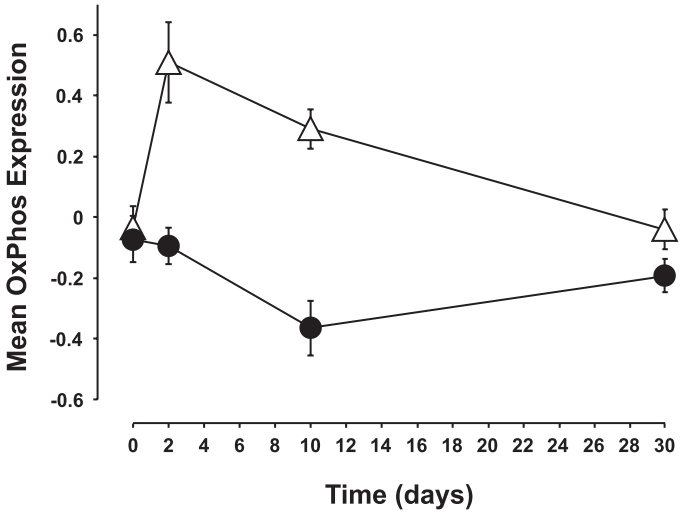

FIG. 3. Coordinated upregulation of OxPhos genes in HFD-fed AJ mice. Mean fold-change over time for 64 OxPhos genes in HFD-fed AJ mice (△) compared with B6 mice (●). The *y*-axis is the mean centroid OxPhos fold-change averaged over six mice per time point. Gene expression measurements were at 0, 2, 10, and 30 days.

transport and oxidative phosphorylation (indicated by a box in Fig. 2). In contrast, HFD-fed B6 mice showed a lower number of enriched mitochondrial-related gene sets. For these mice, out of a total of 12 enriched gene sets, only 3 are related to mitochondrial function, and none of these are for oxidative phosphorylation or electron transport (Fig. 2). For HFD-fed AJ mice, the gene expression profile associated with the enriched mitochondrial gene sets is a transient upregulation of expression at days 2 and 10 followed by a downregulation at day 30 (Fig. 2). A list of all gene sets significantly enriched in either AJ or B6 mice is provided as Supplementary Table 2.

To investigate whether this effect was general across all OxPhos genes, we identified all OxPhos genes present on the cDNA array and measured the mean expression fold-change in HFD versus NC for each mouse strain at each time point (see RESEARCH DESIGN AND METHODS for details). Figure 3 is a plot of the mean fold-change of 64 OxPhos genes in AJ versus B6 mice. Remarkably, the expression profile of B6 mice is opposite that of AJ, showing coordinate downregulation at day 10 compared with coordinate upregulation at days 2 and 10 in AJ mice. Previous studies have implicated peroxisome proliferator–activated receptor γ coactivator (PGC)-1α in the coordinate regulation of OxPhos genes in human diabetes (13). Interestingly, PGC-1α expression levels were transiently upregulated in B6 mice at day 2 (Supplementary Fig. 1), but this was not correlated with an induction of OxPhos genes in these mice. In contrast, in AJ mice, OxPhos genes were increased but no change in PGC-1α could be detected. Postranslational modifications are known to regulate PGC-1α activity (16) and may be responsible for the lack of correlation between its mRNA level and OxPhos gene expression.

In order to further confirm that the whole respiratory chain was differentially regulated, we selected 13 of the most significantly regulated OxPhos genes (Table 1) and categorized them into the different respiratory complexes to which they are associated. The results (Fig. 4) show that the affected genes are associated with all respiratory chain complexes except complex II, which was not present on the array.

Collectively, our data suggest that resistance to HFD-induced hepatosteatosis in AJ mice is associated with a transient adaptation of mitochondrial oxidative phosphorylation activity, possibly increasing mitochondrial respiration.

Increased mitochondrial respiration and uncoupling in AJ mouse livers. To test the hypothesis that mitochondrial respiration is different between B6 and AJ mice, oxygen consumption and ATP production were measured using liver mitochondria at baseline (day 0) and after 10 days of NC diet or HFD when OxPhos gene expression levels are maximally induced in the AJ mouse livers. Measurements were made using either succinate as substrate in the presence of rotenone (SR substrate) or PC.

Data in Fig. 5 show basal respiration (state 2), maximal ADP-stimulated respiration (state 3), and uncoupled respiration (stage 4) for measurements performed with succinate/rotenone. After 10 days of NC diet, all measurements show a significant increase in oxygen consumption in mitochondria from AJ as compared with B6 mouse livers. This strain difference is amplified when the mice are fed an HFD, with B6 mitochondria showing a tendency for a decrease, whereas AJ mitochondria show a significant increase in oxygen consumption.

TABLE 1
Electron transport genes identified by time-course GSEA

Gene symbol	Name	MGI identifier	Correlation
Cycs	cytochrome c, somatic	MGI:88578	−0.29
Atp5k	ATP synthase, H^+ transporting, mitochondrial F1F0 complex, subunit e	MGI:106636	−0.36
Uqcrh	ubiquinol-cytochrome c reductase hinge protein	MGI:1913826	−0.47
Atp5j2	ATP synthase, H^+ transporting, mitochondrial F0 complex, subunit F2	MGI:1927558	−0.48
ATP5 L	ATP synthase, H^+ transporting, mitochondrial F0 complex, subunit g	MGI:1351597	−0.52
Cox4i1	cytochrome c oxidase subunit IV isoform 1	MGI:88473	−0.56
Ndufa8	NADH dehydrogenase (ubiquinone) 1 α subcomplex, 8	MGI:1915625	−0.59
Cyc1	cytochrome c-1	MGI:1913695	−0.7
Uqcrb	ubiquinol-cytochrome c reductase binding protein	MGI:1914780	−0.73
Cox7c	cytochrome c oxidase, subunit VIIc	MGI:103226	−0.77
Cox6a1	cytochrome c oxidase, subunit VI a, polypeptide 1	MGI:103099	−0.8
Cox6c	cytochrome c oxidase, subunit VIc	MGI:104614	−0.84
Ndufc1	NADH dehydrogenase (ubiquinone) 1, subcomplex unknown, 1	MGI:1913627	−0.95

The Pearson correlation value for each gene with the prototype expression profile (see Fig. 1) is shown. Gene names and Mouse Genome Informatics (MGI) accession numbers are from MGI.

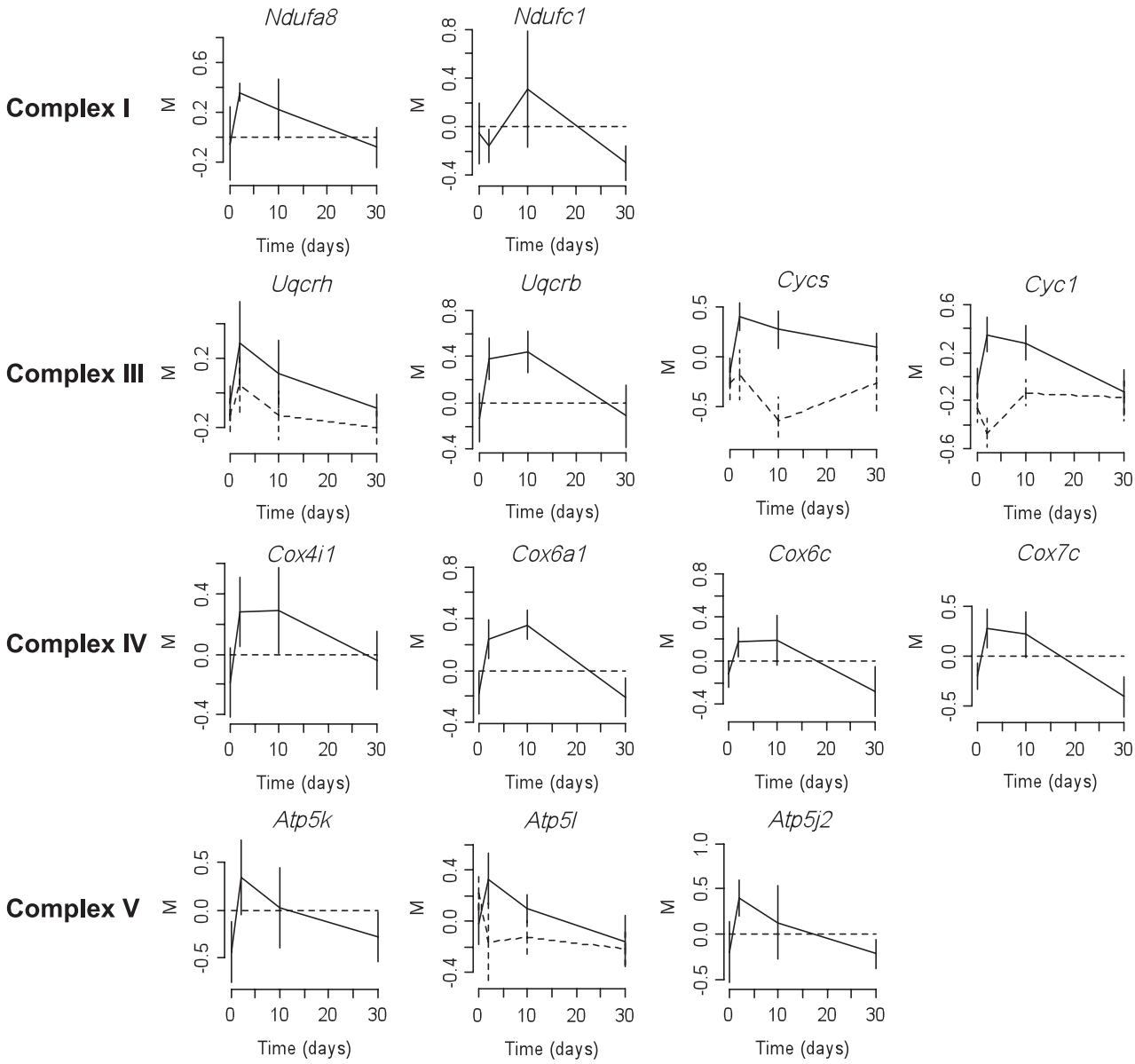

FIG. 4. Individual expression pattern of leading edge genes of the OxPhos gene set during HFD time course in AJ and B6 mice. The genes are classified according to the respiratory chain complex to which they belong: AJ (solid line) and B6 (dotted line). M values correspond to $\log_2$ intensity ratios (HFD/NC for each time point).

Parallel measurements of ATP synthesis rates showed no difference between B6 and AJ mitochondria at any time point. In contrast, there was a progressive reduction in the ATP to oxygen ratio in AJ mouse liver mitochondria that becomes significantly different from that of B6 mitochondria after 10 days of NC and even more important after 10 days of HFD feeding. This further indicates increased uncoupling of AJ mitochondria. In keeping with the restricted expression of uncoupling protein-2 in Kupffer cells (17), we could not detect any increase in liver uncoupling protein-2 expression, as assessed by quantitative RT-PCR analysis (not shown).

When PC was used as a substrate, the same relative increase in oxygen consumption in mitochondria from AJ, as compared with B6 mice was observed after 10 days of NC or HFD feeding. Similarly, the ATP production was identical in all mitochondrial preparations but the AJ mitochondria also showed progressive uncoupling (Fig. 6).

Together the above data indicated an identical capacity for ATP production by liver mitochondria of both strains of mice in each feeding condition. However, mitochondria of AJ mice show an age-dependent, HFD-induced increase in uncoupling. This adaptation of the oxidative phosphorylation chain provides a means to increase energy expenditure in the liver of AJ mice.

DISCUSSION

Time-dependent gene set enrichment analysis revealed a coordinate increase of 13 OxPhos genes, belonging to respiration complexes I, III, IV, and V, in the livers of HFD-fed AJ but not B6 mice. Biochemical analysis confirmed higher mitochondrial respiration rates in the livers

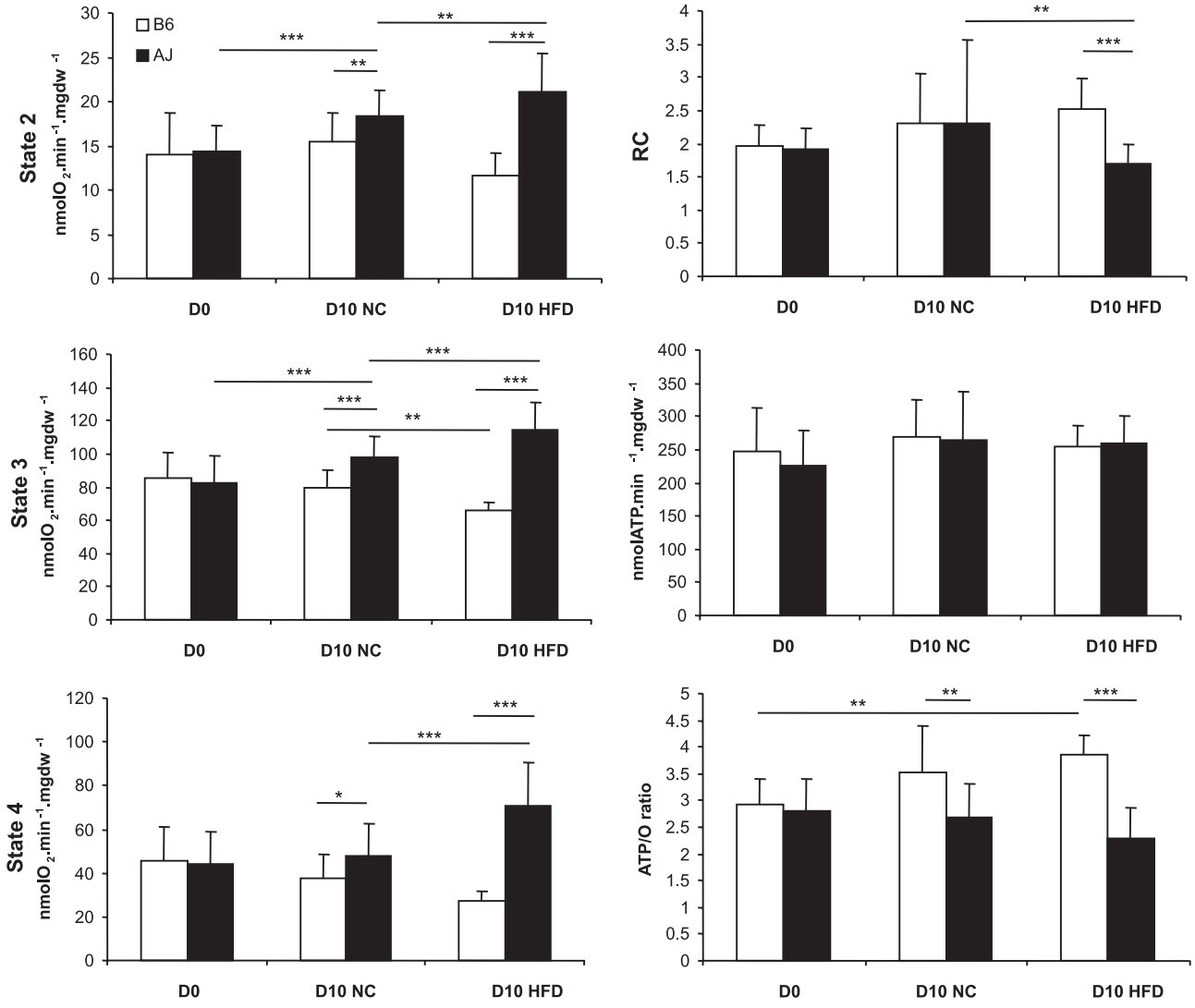

FIG. 5. Mitochondrial respiration using succinate as a substrate (SR). B6 (open bars) and AJ (filled bars) mouse liver mitochondria were compared at baseline (d = 0) or after 10 days of NC (D10 NC) or HFD feeding (D10 HFD). State 2, respiration in the absence of ADP; state 3, ADP (1 nmol/L)-stimulated respiration; state 4, oligomycin (1 mg/mL)-inhibited respiration; RC, respiratory control ratio (state 3/state 4); ATP, ATP synthesis rate in state 3; ATP/O, ATP produced per oxygen consumed; mgdw, milligrams of dry weight. Values are shown as mean ± SD, $n = 6$. *$P < 0.05$; **$P < 0.01$; ***$P < 0.001$.

of AJ mice as well as marked uncoupling of mitochondrial respiration. These data demonstrate flexibility in the expression of the OxPhos genes in AJ mice in response to an acute increase in energy intake. This response may protect against the initial deleterious effect of HFD feeding by increasing energy dissipation and reducing reactive oxygen species production. It is part of a global protective response of the AJ mouse livers to HFD, which involves several lipid metabolic pathways, as previously described (8).

GSEA results are usually difficult to confirm by direct quantitative analysis of gene expression because this statistical technique searches for groups of genes that belong to a given biological pathway and whose expression is coordinately regulated even though each individual gene may not be statistically differentially regulated between two conditions. Therefore, we did not attempt to confirm changes in mRNA expression by quantitative methods, but instead we measured mitochondrial respiration and ATP synthesis in mitochondria prepared from the livers of NC or HFD-fed AJ and B6 mice. Consistent with the GSEA analysis, we detected an increase in mitochondrial respiration in livers of AJ mice fed an HFD for 10 days.

A number of recent studies found a coordinately decreased expression of OxPhos genes in muscles (18–20), livers, and fat (21–23) of diabetic patients, leading to the suggestion that a reduced oxidative phosphorylation capacity can favor diabetes development. In contrast, in one study (24), an increase in OxPhos gene expression was observed in the livers of obese patients with type 2 diabetes and this was correlated with increased measures of insulin resistance and diabetes. Thus, it is unclear whether changes in OxPhos gene expression cause disease progression or are a compensatory response to the diseased state. Studies in mice with muscle or liver-specific inactivation of the apoptosis-inducing factor (*AIF*) gene, which reduces OxPhos activity as found in human patients, showed increased insulin sensitivity and resistance to diet-induced obesity (23). The proposed explanation for this unanticipated observation is that reduced ATP production, as well as increased intracellular AMP

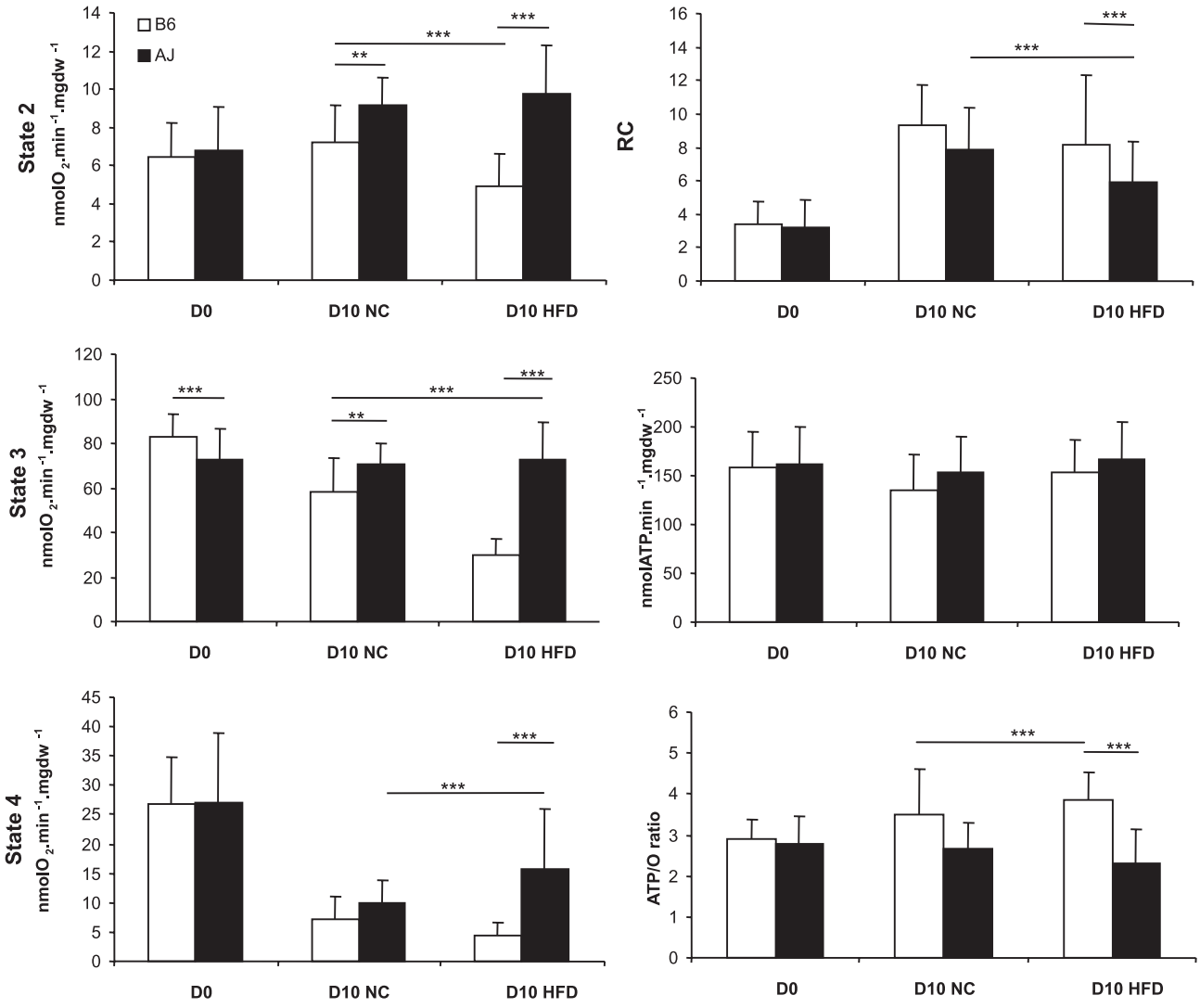

FIG. 6. Mitochondrial respiratory parameters using the substrate PC. B6 (open bars) and AJ (filled bars) mice were compared at baseline (d = 0) or after 10 days of NC (D10 NC) or HFD feeding (D10 HFD). State 2, respiration in the absence of ADP; state 3, ADP (1 nmol/L)-stimulated respiration; state 4, oligomycin (1 mg/mL)-inhibited respiration; RC, respiratory control ratio (state 3/state 4); ATP, ATP synthesis rate in state 3; ATP/O, ATP produced per oxygen consumed; mgdw, milligrams of dry weight. Values are shown as mean ± SD, $n = 6$. *$P < 0.05$; **$P < 0.01$; ***$P < 0.001$.

levels, stimulates glucose utilization and fatty acid oxidation, thereby favoring nutrient absorption and catabolism. In both cases, however, it is difficult to assess the contribution of reduced OxPhos genes in the susceptibility to obesity or diabetes. Indeed, in the human studies, analysis has been performed at a single time point in the disease history of each patient and thus a possible causative role cannot be assessed. In the AIF knockout mice, the changes in OxPhos gene expression are induced early in the life of the animal and may induce unidentified compensatory mechanisms.

Our present study reveals a different aspect of OxPhos gene-regulated expression: its capacity to be rapidly and transiently increased in response to HFD feeding in mice that are protected against hepatic steatosis and obesity. This is also associated with increased mitochondrial uncoupling, which probably reduces the production of superoxide anions generated by electrons leaking from the OxPhos chain (25–27) and which can induce oxidative damage in the liver of AJ mice. In this context, results from our recent study (8) indicated that upon HFD feeding, expression of mitochondrial β-oxidation genes was increased in B6 but not AJ mouse livers. Thus, in response to fatty acid overload, more reduced nucleotides may be produced and channeled to the OxPhos chain in B6 mouse livers, but in the absence of an increased capacity to generate ATP or to uncouple mitochondria, this must further favor reactive oxygen species production (28). Together, our observations suggest that upon initiation of HFD, the B6 mouse livers are prone to induction of ROS damage, whereas reduced efficiency of ATP generation in AJ mouse livers helps to utilize the excess of substrates while balancing ATP supply with cellular energy requirements (29,30).

Adaptation of mice to HFD proceeds in different phases with considerable up- or downregulation of many genes in the first days of HFD, followed by a slow return of many genes to their basal levels of expression, with some gene expression levels remaining permanently modified (10,31–33). In our previous study of AJ and B6 mouse liver adaptation to an HFD, we identified a rapid and coordinate increase in the expression of 10 peroxisomal genes, a microsomal elongase (*Elovl5*), and two microsomal

desaturases (*Fads1* and *Fads2*) (8). This was associated with increased peroxisomal β-oxidation activity and increased production of the cannabinoid receptor agonist 2-AG, whose production from n-6 unsaturated fatty acids is favored by the action of the microsomal enzymes. Thus, in AJ mouse livers, there is a rapid adaptation of several metabolic pathways to HFD: *1*) increased peroxisomal β-oxidation; *2*) increased n-3 and n-6 fatty acid detoxification by desaturation and conversion to bioactive, protective lipids such as 2-AG; and, as shown in the current study, *3*) increased OxPhos and mitochondrial uncoupling. Collectively, these observations indicate that resistance to HFD-induced hepatic steatosis in AJ mouse livers and possible protection against obesity development is favored by the rapid adaptation of multiple metabolic pathways that protect the liver against a toxic lipid overload.

The participation of several pathways in resistance against diet-induced hepatosteatosis and obesity is consistent with analysis of mouse chromosome substitution lines that showed that AJ chromosomal loci able to protect B6 mice against diet-induced obesity were present in at least 17 different chromosomes (34). Whether any of the pathways mentioned above has a dominant role in the development of hepatosteatosis and obesity is not clear. Studies with mice engineered to change the expression level or activity of any of these pathways could shed light on this question. Nevertheless, these studies suggest that the ability of an organ to rapidly adapt to changes in nutrient availability is an important aspect of the protective response to a metabolic stress and clearly show that this response is genetically encoded, although epigenetic programming may also be involved (10,32,33). These studies also suggest that the ability to regulate gene expression may be as important as changes in protein structure and/or function in determining the susceptibility to metabolic diseases. This proposal is clearly in agreement with genome-wide association studies that usually find disease susceptibility variants in noncoding regions, which may impact gene transcription activity (35). This is also reminiscent of the metabolic inflexibility hypothesis that proposes that a key defect in obesity and type 2 diabetes is a reduced capacity to switch from the use of glucose to lipid as oxidative substrates during the fed to postabsorptive phase (36,37). Thus, long-term development of metabolic diseases may be associated with failure to acutely adapt metabolic pathways to a change in nutrient availability. Thus, we propose that the concept of metabolic flexibility be extended to include the capacity of organs, such as livers, to rapidly adapt their metabolic pathways to prevent transient generation of damaging metabolites that, over time, can accumulate to create pathological conditions.

ACKNOWLEDGMENTS

This work was supported by grants from the Swiss National Science Foundation (3100A0-113525), the Swiss SystemsX.ch initiative, LipidX-2008/011, and the European Union Sixth Framework Program on Hepatic and Adipose Tissue and Functions in the Metabolic Syndrome (EU-FP6 HEPADIP) to B.T. E.D.A. is supported by National Institutes of Health Grant UO1-HL-087947.

No potential conflicts of interest relevant to this article were reported.

C.P. performed bioinformatic analysis. M.I. performed bioinformatic analysis and wrote the manuscript. D.H. contributed microarray data. J.D. and J.S. contributed experimental data. E.D.A. and B.T. designed experiments and wrote the manuscript.

REFERENCES

1. Postic C, Girard J. Contribution of de novo fatty acid synthesis to hepatic steatosis and insulin resistance: lessons from genetically engineered mice. J Clin Invest 2008;118:829–838
2. Cai D, Yuan M, Frantz DF, et al. Local and systemic insulin resistance resulting from hepatic activation of IKK-beta and NF-kappaB. Nat Med 2005;11:183–190
3. de Luca C, Olefsky JM. Inflammation and insulin resistance. FEBS Lett 2008;582:97–105
4. Hotamisligil GS. Inflammation and metabolic disorders. Nature 2006;444:860–867
5. Sethi JK, Vidal-Puig AJ. Thematic review series: adipocyte biology. Adipose tissue function and plasticity orchestrate nutritional adaptation. J Lipid Res 2007;48:1253–1262
6. Biddinger SB, Hernandez-Ono A, Rask-Madsen C, et al. Hepatic insulin resistance is sufficient to produce dyslipidemia and susceptibility to atherosclerosis. Cell Metab 2008;7:125–134
7. Surwit RS, Feinglos MN, Rodin J, et al. Differential effects of fat and sucrose on the development of obesity and diabetes in C57BL/6J and A/J mice. Metabolism 1995;44:645–651
8. Hall D, Poussin C, Velagapudi VR, et al. Peroxisomal and microsomal lipid pathways associated with resistance to hepatic steatosis and reduced pro-inflammatory state. J Biol Chem 2010;285:31011–31023
9. Chomczynski P, Sacchi N. Single-step method of RNA isolation by acid guanidinium thiocyanate-phenol-chloroform extraction. Anal Biochem 1987;162:156–159
10. De Fourmestraux V, Neubauer H, Poussin C, et al. Transcript profiling suggests that differential metabolic adaptation of mice to high fat diet is associated with changes in liver to muscle lipid fluxes. J Biol Chem 2004;279:50743–50753
11. Gentleman RC, Carey VJ, Bates DM, et al. Bioconductor: open software development for computational biology and bioinformatics. Genome Biol 2004;5:R80
12. Subramanian A, Tamayo P, Mootha VK, et al. Gene set enrichment analysis: a knowledge-based approach for interpreting genome-wide expression profiles. Proc Natl Acad Sci USA 2005;102:15545–15550
13. Mootha VK, Lindgren CM, Eriksson KF, et al. PGC-1alpha-responsive genes involved in oxidative phosphorylation are coordinately downregulated in human diabetes. Nat Genet 2003;34:267–273
14. O'Neill BT, Kim J, Wende AR, et al. A conserved role for phosphatidylinositol 3-kinase but not Akt signaling in mitochondrial adaptations that accompany physiological cardiac hypertrophy. Cell Metab 2007;6:294–306
15. Zhang Y, Soto J, Park K, et al. Nuclear receptor SHP, a death receptor that targets mitochondria, induces apoptosis and inhibits tumor growth. Mol Cell Biol 2010;30:1341–1356
16. Cantó C, Auwerx J. PGC-1alpha, SIRT1 and AMPK, an energy sensing network that controls energy expenditure. Curr Opin Lipidol 2009;20:98–105
17. Larrouy D, Laharrague P, Carrera G, et al. Kupffer cells are a dominant site of uncoupling protein 2 expression in rat liver. Biochem Biophys Res Commun 1997;235:760–764
18. Lowell BB, Shulman GI. Mitochondrial dysfunction and type 2 diabetes. Science 2005;307:384–387
19. Wisløff U, Najjar SM, Ellingsen O, et al. Cardiovascular risk factors emerge after artificial selection for low aerobic capacity. Science 2005;307:418–420
20. Rabøl R, Boushel R, Dela F. Mitochondrial oxidative function and type 2 diabetes. Appl Physiol Nutr Metab 2006;31:675–683
21. Dahlman I, Forsgren M, Sjögren A, et al. Downregulation of electron transport chain genes in visceral adipose tissue in type 2 diabetes independent of obesity and possibly involving tumor necrosis factor-alpha. Diabetes 2006;55:1792–1799
22. Misu H, Takamura T, Matsuzawa N, et al. Genes involved in oxidative phosphorylation are coordinately upregulated with fasting hyperglycaemia in livers of patients with type 2 diabetes. Diabetologia 2007;50:268–277
23. Pospisilik JA, Knauf C, Joza N, et al. Targeted deletion of AIF decreases mitochondrial oxidative phosphorylation and protects from obesity and diabetes. Cell 2007;131:476–491

24. Takamura T, Misu H, Matsuzawa-Nagata N, et al. Obesity upregulates genes involved in oxidative phosphorylation in livers of diabetic patients. Obesity (Silver Spring) 2008;16:2601–2609
25. Boss O, Hagen T, Lowell BB. Uncoupling proteins 2 and 3: potential regulators of mitochondrial energy metabolism. Diabetes 2000;49:143–156
26. Horimoto M, Fülöp P, Derdák Z, Wands JR, Baffy G. Uncoupling protein-2 deficiency promotes oxidant stress and delays liver regeneration in mice. Hepatology 2004;39:386–392
27. Nègre-Salvayre A, Hirtz C, Carrera G, et al. A role for uncoupling protein-2 as a regulator of mitochondrial hydrogen peroxide generation. FASEB J 1997;11:809–815
28. Chance B, Sies H, Boveris A. Hydroperoxide metabolism in mammalian organs. Physiol Rev 1979;59:527–605
29. Chavin KD, Yang S, Lin HZ, et al. Obesity induces expression of uncoupling protein-2 in hepatocytes and promotes liver ATP depletion. J Biol Chem 1999;274:5692–5700
30. Tsuboyama-Kasaoka N, Sano K, Shozawa C, Osaka T, Ezaki O. Studies of UCP2 transgenic and knockout mice reveal that liver UCP2 is not essential for the antiobesity effects of fish oil. Am J Physiol Endocrinol Metab 2008; 294:E600–E606
31. Burcelin R, Crivelli V, Dacosta A, Roy-Tirelli A, Thorens B. Heterogeneous metabolic adaptation of C57BL/6J mice to high-fat diet. Am J Physiol Endocrinol Metab 2002;282:E834–E842
32. Poussin C, Hall D, Minehira K, Galzin AM, Tarussio D, Thorens B. Different transcriptional control of metabolism and extracellular matrix in visceral and subcutaneous fat of obese and rimonabant treated mice. PLoS ONE 2008;3:e3385
33. Koza RA, Nikonova L, Hogan J, et al. Changes in gene expression foreshadow diet-induced obesity in genetically identical mice. PLoS Genet 2006;2:e81
34. Singer JB, Hill AE, Burrage LC, et al. Genetic dissection of complex traits with chromosome substitution strains of mice. Science 2004;304: 445–448
35. Gaulton KJ, Nammo T, Pasquali L, et al. A map of open chromatin in human pancreatic islets. Nat Genet 2010;42:255–259
36. Kelley DE, Mandarino LJ. Fuel selection in human skeletal muscle in insulin resistance: a reexamination. Diabetes 2000;49:677–683
37. Mandarino LJ, Consoli A, Jain A, Kelley DE. Interaction of carbohydrate and fat fuels in human skeletal muscle: impact of obesity and NIDDM. Am J Physiol 1996;270:E463–E470